Monocular inspection of spacecraft under illumination constraints and avoidance regions

Tochukwu Elijah Ogri[1] Muzaffar Qureshi[1] Zachary I. Bell[2] Matthew Longmire[3] Rushikesh Kamalapurkar[1]

***Abstract*— This paper presents an adaptive control approach to information-based guidance and control of a spacecraft carrying out on-orbit inspection by actively computing optimal policies for the spacecraft to achieve the best possible representation of objects within its orbital environment. Due to the complexity of navigating the space environment, it may be impossible to carry out on-orbit servicing to maintain space systems like satellites using a spacecraft equipped with controllers that cannot adapt to changing conditions. In particular, the presence of constraints such as illumination, field-of-view (FOV), minimal fuel, the use of visual-inertial navigation for improved localization, and the need for real-time computation of control policies render the spacecraft motion planning problem challenging. The control framework developed in this paper addresses these challenges by formulating the inspection task as a constrained optimization problem where the goal is to maximize information gained from the cameras, while navigating to the *next best view*, subject to illumination and FOV constraints. The developed architecture is analyzed using a Lyapunov-based stability analysis and the effectiveness of the planning algorithm is verified in simulation.**

I. Introduction Review

In autonomous tasks such as on-orbit inspection and GPS-denied navigation, onboard sensors are utilized to generate a local map of the environment and also to localize agents relative to objects in the local map [1]. While effective algorithms for localization and mapping have been developed over the past few decades [2], the problem of motion planning to improve localization and mapping performance in the presence of complex constraints in the operating environment still presents some open questions [3]–[10].

Prior research on satellite inspection and relative orbital control include [3], [8], where the authors developed an information-based guidance and control framework for inspecting and mapping a chief satellite using multiple deputy spacecraft in stable passive relative orbits (PROs). The authors utilize an optimal control formulation that employs a popular Bayesian-based information cost (see [11], [12]) to maximize the information content of an image acquired by the camera attached to each deputy. This Bayesian metric, while suitable for inspection tasks where the deputy has a localization system independent of the camera, is not suitable if the pose of the deputy spacecraft relative to the chief satellite must also be estimated using the same camera being used for inspection. If the camera is shared by the inspection and localization systems, then information gain heavily depends on the motion of the camera, and as such, cannot be measured using a single image.

Another approach for vision-based navigation and control is presented in [13], where a multiplicative extended Kalman filter is used for relative pose estimation via photogrammetry. Similarly, [5] employs an unscented Kalman filter for pose estimation and shape reconstruction using images from a single camera and a range finder. Recently, reinforcement learning-based control techniques [7], [9] have also been applied to satellite inspection, where the authors use Proximal Policy Optimization deep reinforcement learning to control a single free-flying deputy spacecraft equipped with an optical sensor to inspect a chief satellite. However, since their controller is trained offline, it limits its applicability in debris-riddled space environments where real-time adaptive control is essential.

Most of the methods outlined above rely on exact knowledge of the shape and the motion of the target spacecraft so that they can carry out their space tasks. In this paper, pixel coordinates of features on the chief satellite are fed into an integral concurrent learning (ICL)-based observer which estimates the relative distances to these features to create a local map of the environment for relative navigation. To carry out the inspection task, this map is fed to an adaptive optimal control-based planning and control algorithm for maximizing information gain from a camera fixed to the deputy spacecraft. Information gain maximization in this paper refers to improving the conditioning of the regressor of the ICL-based observer by integrating a new and dynamic information gain metric that is based on sequences of images into the cost function of an optimal control problem and solution of the said problem under realistic FOV constraints. This paper employs K-means clustering to determine which features of the chief satellite require subsequent inspection and adaptive optimal control to maximize information gain along the trajectory while visiting these inspection points.

II. Problem Formulation

A. Spacecraft Motion Model

The center of mass of the deputy spacecraft, $\mathcal{O}_{\mathcal{B}}$, is the origin of the body frame, $\mathcal{F}_{\mathcal{B}}$, with the basis $\{\vec{x}_B, \vec{y}_B, \vec{z}_B\}$. The spacecraft has a camera for inspecting points on a

This research was supported in part by the Air Force Research Laboratories under contract numbers FA8651-24-1-0019 and FA8651-23-1-0006. Any opinions, findings, or recommendations in this article are those of the author(s), and do not necessarily reflect the views of the sponsoring agencies.

[1] Department of Mechanical and Aerospace Engineering, University of Florida, Gainesville, Florida, USA, email: {tochukwu.ogri, muzaffar.qureshi, rkamalapurkar} @ufl.edu.

[2] Air Force Research Laboratories, Florida, USA, email: zachary.bell.10@us.af.mil.

[3] Autonomous Vehicles Laboratory, University of Florida, Gainesville, Florida, USA, email: m.longmire@ufl.edu.

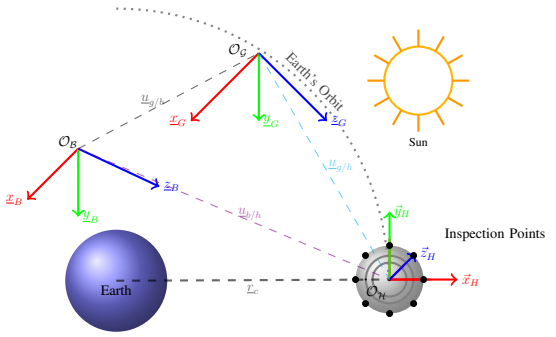

Fig. 1. Illustration of the relative position of the deputy spacecraft, chief satellite, and the goal location in Hill's Reference Frame.

satellite. For ease of exposition, the camera is assumed to be fixed in $\mathcal{F}_{\mathcal{B}}$. Optimization using a gimbled camera is a part of ongoing research . The dynamics of the relative motion between the deputy spacecraft and the chief satellite are represented in Hill's reference frame $\mathcal{F}_{\mathcal{H}}$ illustrated in Figure 1, with the basis $\{\vec{x}_H, \vec{y}_H, \vec{z}_H\}$ and the origin $\mathcal{O}_{\mathcal{H}}$ centered on the chief satellite moving in a circular orbit around the earth. The unit vector $\vec{x}_H$ is aligned with the line joining the center of the Earth and $\mathcal{O}_{\mathcal{H}}$, directed away from the Earth, $\vec{y}_H$ points in the tangential direction of the motion of the chief satellite, and $\vec{z}_H$-axis completes the right-handed basis. Finally, let $\mathcal{F}_{\mathcal{G}}$ represent a goal frame that has its origin at the goal, $\mathcal{O}_{\mathcal{G}}$, and the basis $\{\vec{x}_G, \vec{y}_G, \vec{z}_G\}$. The control objective is to drive the deputy spacecraft to the goal location while maximizing information gain from the camera, in the sense made precise in Section IV.

B. Satellite dynamics

To describe the relative dynamics between the chief satellite and deputy spacecraft, it is assumed that the chief satellite is in a near-circular orbit around the earth so that the angular velocity of the Hill's reference frame is equivalent to the orbital rate of the chief satellite. In addition, it is assumed that the chief satellite and the deputy spacecraft start close to each other, in near-synchronous orbits so that only small maneuvers are needed to achieve relative navigation. Under these conditions and assuming a near-spherical Earth, the relative motion between the deputy spacecraft and chief satellite can be described using the Clohessy-Wiltshire (CW) equations,

$$(\dot{\underline{v}}_{b/h}(t))_x = 2n(\underline{v}_{b/h}(t))_y + 3n^2(\underline{p}_{b/h}(t))_x + \frac{(F)_x}{m}, \quad (1)$$

$$(\dot{\underline{v}}_{b/h}(t))_y = -2n(\underline{v}_{b/h}(t))_x + \frac{(F)_y}{m}, \quad (2)$$

$$(\dot{\underline{v}}_{b/h}(t))_z = -n^2(\underline{p}_{b/h}(t))_z + \frac{(F)_z}{m}, \quad (3)$$

where $\underline{p}_{b/h}(t)$ and $\underline{v}_{b/h}(t)$ represent the relative position and velocity of the deputy spacecraft relative to the chief satellite, respectively, coordinatized in $\mathcal{F}_{\mathcal{H}}$, $n = \frac{\mu}{r_0^3}$ is the mean motion of the chief satellite, μ is Earth's gravitational constant, $F \in \mathbb{R}^3$ is the net force applied by the thrusters on the center of mass of the deputy, r_0 is the radius of the orbit of the chief satellite, and m is the mass of the deputy spacecraft.

C. Motion Model of the camera

The following assumptions facilitate the development of a model of the camera attached to the deputy spacecraft.

Assumption 1: The chief satellite has features, $i = 1, \ldots, N$, where $N > 0$, that can be identified, provided they are within the field-of-view (FOV) of the camera and are illuminated by the Sun. Additionally, the shape of the chief satellite is spherical.

Assumption 2: The intrinsic matrix of the camera, $\mathbf{A} \in \mathbb{R}^{3\times3}$, is known and invertible [14]. In particular, the unit vector $\underline{u}_{b/h}(t) \in \mathbb{R}^3$ can be obtained from $\underline{u}_{b/h}(t) := \frac{\mathbf{A}^{-1}P_{b/h}(t)}{\left\|\mathbf{A}^{-1}P_{b/h}(t)\right\|}$ where $P_{b/h}(t)$ are the measured pixel coordinates of the chief satellite relative to the deputy spacecraft in $\mathcal{F}_{\mathcal{H}}$ represented as homogeneous coordinates.

Remark 1: Assumption 1–2 enable the use of feature extraction techniques like those described in [15], [16] to extract features from images of the chief satellite while they are within the FOV of the camera and illuminated by the sun.

Under Assumptions 1–2 the positions of the deputy, goal, and chief relative to each other can be expressed as

$$\underline{p}_{b/h}(t) - \underline{p}_{g/b}(t) = \underline{p}_{g/h}, \quad (4)$$

where $\underline{p}_{g/b}(t) \in \mathbb{R}^3$ represents the position of the goal relative to the deputy, coordinatized in $\mathcal{F}_{\mathcal{H}}$ and $\underline{p}_{g/h} \in \mathbb{R}^3$ is the position of the goal relative to the chief satellite, coordinatized in $\mathcal{F}_{\mathcal{H}}$. Given that $\underline{p}_{b/h}(t) = \underline{u}_{b/h}(t)\underline{d}_{b/h}(t)$, $\underline{p}_{g/b}(t) = \underline{u}_{g/b}(t)\underline{d}_{g/b}(t)$, and $\underline{p}_{g/h} = \underline{u}_{g/h}\underline{d}_{g/h}$, where the scalars $\underline{d}_{b/h}(t) > 0$, $\underline{d}_{g/b}(t) > 0$, and $\underline{d}_{g/h} > 0$ are the unknown Euclidean distances between the deputy spacecraft, the goal, and the chief satellite, the expression in (4) can be equivalently written as

$$\begin{bmatrix}\underline{u}_{b/h}(t) & -\underline{u}_{g/b}(t)\end{bmatrix}\begin{bmatrix}\underline{d}_{b/h}(t)\\ \underline{d}_{g/b}(t)\end{bmatrix} = \underline{u}_{g/h}\underline{d}_{g/h}. \quad (5)$$

The unit vector $\underline{u}_{b/h}(t)$ is calculated using Assumptions 2 and $\underline{u}_{g/b}(t) = \frac{\underline{p}_{g/b}(t)}{\left\|\underline{p}_{g/b}(t)\right\|}$. The unit vector pointing from the nearest cluster of uninspected points on the chief satellite to the goal, $\underline{u}_{g/h} \in \mathbb{R}^3$, is determined through k-means clustering algorithm [17]. The k-means clustering algorithm serves as a high-level planner, identifying the nearest cluster of uninspected points within the FOV of the camera. The goal location is then selected to lie at a fixed distance from the chief satellite along the goal unit vector. This unit vector is piecewise constant, implying that $\underline{p}_{g/h}$ in (4) is also piecewise constant. This goal selection algorithm ensures that the deputy only moves towards the nearest cluster of uninspected illuminated points.

Assumption 3: The linear velocity of the camera relative to the chief satellite, $\underline{v}_{b/h}(t)$, coordinatized in $\mathcal{F}_{\mathcal{H}}$, is measurable.

Under Assumptions 2 and 3, the time derivatives of the unknown distances are known and given by

$$\begin{bmatrix} \dot{\underline{d}}_{b/h}(t) \\ \dot{\underline{d}}_{g/b}(t) \end{bmatrix} = \begin{bmatrix} \underline{u}_{b/h}{}^{\top}(t) \\ \underline{u}_{g/b}{}^{\top}(t) \end{bmatrix} \underline{v}_{b/h}(t) \text{ and } \dot{\underline{d}}_{g/h} = 0. \quad (6)$$

III. ICL Based Observer Update Laws For Estimating Euclidean Distances

To estimate the unknown Euclidean distances $\underline{d}_{b/h}(t)$, $\underline{d}_{g/b}(t)$, and $\underline{d}_{g/h}$, distance observers will be designed in this section using ICL. Stacking (5) for every feature $i = 1, \dots N$ of the chief yields the expression

$$\theta_1(t) = Y(t)\theta_2 \quad (7)$$

where $Y(t) = \left(Y_1^{\top}(t)Y_1(t)\right)^{-1} Y_1^{\top}(t)Y_2 \in \mathbb{R}^{(N+1)\times N}$, $Y_1(t) \coloneqq \begin{bmatrix} \text{diag}(\underline{u}_{b/1}(t) \ \dots \ \underline{u}_{b/N}(t)) & -\underline{u}_{g/b}(t)\cdot \mathbf{1}_{N\times 1} \end{bmatrix} \in \mathbb{R}^{3N\times(N+1)}$, $Y_2 \coloneqq \text{diag}(\underline{u}_{g/1} \ \dots \ \underline{u}_{g/N}) \in \mathbb{R}^{3N\times N}$, $\theta_1(t) \coloneqq \begin{bmatrix} \underline{d}_{b/1}(t) & \dots & \underline{d}_{b/N}(t) & \underline{d}_{g/b}(t) \end{bmatrix}^{\top} \in \mathbb{R}^{N+1}$, $\theta_2 \coloneqq \begin{bmatrix} \underline{d}_{g/1} & \dots & \underline{d}_{g/N} \end{bmatrix}^{\top} \in \mathbb{R}^N$, and $\text{diag}(\cdot)$ denotes a block diagonal matrix. $Y_1(t)$ is full rank provided the origin of the camera is not coincident with the origin of the goal at $t = 0$. Similarly, stacking the dynamics in (6) for every feature $i = 1, \dots, N$, and integrating the resulting expression over a time delay $\Delta t \in [0,\ t_f)$, (cf. [18], [19])

$$\theta_1(t) - \theta_1(t - \Delta t) = \int_{t-\Delta t}^{t} U(\tau)\underline{v}_{b/h}(\tau)\text{d}\tau, \quad (8)$$

for all $t > \Delta t$, where $U(t) \coloneqq \begin{bmatrix} \underline{u}_{b/1}^{\top}(t) & \dots & \underline{u}_{b/N}^{\top}(t) & \underline{u}_{g/b}^{\top}(t) \end{bmatrix}^{\top} \in \mathbb{R}^{(N+1)\times 3}$. Substituting (8) in (7) yields

$$\mathcal{Y}(t)\theta_2 = \mathcal{U}(t) \quad (9)$$

where $\mathcal{Y}(t) \coloneqq \begin{cases} 0_{(N+1)\times N}, & t \le \Delta t, \\ (Y(t) - Y(t-\Delta t)), & t > \Delta t \end{cases}$ and $\mathcal{U}(t) \coloneqq \begin{cases} 0_{(N+1)\times N}, & t \le \Delta t, \\ \int_{t-\Delta t}^{t} U(\tau)\underline{v}_{b/h}(\tau)\text{d}\tau, & t > \Delta t. \end{cases}$ Multiplying both sides of (9) by $\mathcal{Y}^{\top}(t)$ yields $\mathcal{Y}^{\top}(t)\mathcal{Y}(t)\theta_2 = \mathcal{Y}^{\top}(t)\mathcal{U}(t)$. In general, $\mathcal{Y}(t)$ will not have full column rank (e.g. when the camera is stationary) implying that in general, $\mathcal{Y}^{\top}(t)\mathcal{Y}(t) \succeq 0$. However, the equality may be evaluated at $M > 1$ time instants and summed together as $\left(\sum_{j=1}^{M} \frac{\mathcal{Y}^{\top}(t_j)\mathcal{Y}(t_j)}{1+\|\mathcal{Y}(t_j)\|^2}\right)\theta_2 = \sum_{j=1}^{M} \frac{\mathcal{Y}^{\top}(t_j)\mathcal{U}(t_j)}{1+\|\mathcal{Y}(t_j)\|^2}$, where the denominator term ensures the boundedness of the sum. Let $\Sigma_{\mathcal{Y}}(t) \coloneqq \sum_{j=1}^{M} \frac{\mathcal{Y}^{\top}(t_j)\mathcal{Y}(t_j)}{1+\|\mathcal{Y}(t_j)\|^2}$ and $\Sigma_{\mathcal{U}}(t) \coloneqq \sum_{j=1}^{M} \frac{\mathcal{Y}^{\top}(t_j)\mathcal{U}(t_j)}{1+\|\mathcal{Y}(t_j)\|^2}$. To obtain the estimates of the distances, the following rank condition on the regressor matrix is needed.

Assumption 4: The camera has uniformly sufficiently rich motion, that is, there exist finite constants $T > \Delta t$ and $\underline{\Sigma} > 0$ such that for all initial conditions $\begin{bmatrix} \underline{p}_{b/h}^{\top}(0) & \underline{v}_{b/h}^{\top}(0) & \theta_2^{\top}(0) \end{bmatrix}^{\top} \in \mathbb{R}^{6+N}$ and for all time $t \ge T$, $\lambda_{\min}\left(\Sigma_{\mathcal{Y}}(t)\right) > \underline{\Sigma}$, where $\lambda_{\min}(\cdot)$ and $\lambda_{\max}(\cdot)$ are the minimum and maximum eigenvalues of $(\cdot)$, respectively.

Remark 2: This assumption is an observability condition for the subsequent development that is similar to other image-based observers [18]–[20]. Assumption 4 can be verified online for each trajectory. It only requires excitation over a finite time interval, and as such, is weaker than traditional persistence of excitation (PE) conditions.

The time T is unknown; however, it can be determined online by checking the minimum eigenvalue of the regressor matrix in Assumption 4. While the lower bound in Assumption 4 can be verified for each trajectory, uniformity with respect to initial conditions is impossible to verify. The uniformity assumption can be relaxed in favor of a weaker, per-trajectory bound. Under such a bound, we can obtain a non-uniform ultimate boundedness result instead of the uniform ultimate boundedness result in Theorem 2. For $t \ge T$, $\lambda_{\min}(\Sigma_{\mathcal{Y}}(t)) > \underline{\Sigma}$ implies that the estimate of θ_2 can be computed using the adaptive update law

$$\dot{\hat{\theta}}_2(t) = \begin{cases} 0_{N\times 1}, & t < T, \\ \beta\left(\Sigma_{\mathcal{Y}}^{-1}(t)\Sigma_{\mathcal{U}}(t) - \hat{\theta}_2(t)\right), & t \ge T, \end{cases} \quad (10)$$

where $\hat{\theta}_2(t) \in \mathbb{R}^N$ is the estimate of θ_2 and $\beta \succ 0 \in \mathbb{R}^{N\times N}$ is a constant matrix. Substituting $\hat{\theta}_2(t)$ in (7) yields an estimate of $\theta_1(t)$ given by $\hat{\theta}_1(t) = Y(t)\hat{\theta}_2(t)$. If $\hat{\theta}_2(t)$ converges to θ_2, then $\hat{\theta}_1(t)$ converges to $\theta_1(t)$ because of the relationship in (7). Hence, it is sufficient to prove convergence of $\hat{\theta}_2(t)$ to θ_2.

Remark 3: When features leave the FOV of the camera, it may not be possible to take the pseudoinverse of $Y(t)$ since some of the unit vectors in $Y(t)$ are no longer measurable. To account for features entering or leaving the FOV, the distance estimate for each feature in the FOV can be calculated separately instead of estimating all features at the same time as in (10). In that case, update laws for individual features can be turned off when they leave the FOV and turned back on when they re-enter the FOV. In this paper, for ease of exposition, we consider the case where all N features are in the FOV throughout the experiment.

A. Analysis of the ICL-Based Observer

To analyze the convergence of the ICL-based observer in (10), let the observer error be defined as $\tilde{\theta}_2(t) \coloneqq \theta_2 - \hat{\theta}_2(t)$, with the observer error dynamics given by

$$\dot{\tilde{\theta}}_2(t) = \begin{cases} 0_{N\times 1}, & t < T, \\ -\beta\tilde{\theta}_2(t), & t \ge T. \end{cases} \quad (11)$$

The following theorem establishes the exponential stability of the observer error system in (11).

Theorem 1: Let $V : \mathbb{R}^N \to \mathbb{R}$ be a candidate Lyapunov function defined as $V(\tilde{\theta}_2) = \frac{1}{2}\tilde{\theta}_2^{\top}\tilde{\theta}_2$. Provided Assumptions 1-4 hold, the update law defined in (10) ensure that the origin of the observer error system in (11) is globally exponentially stable and the trajectories of the observer error $\tilde{\theta}_2(\cdot)$ converge exponentially to the origin.

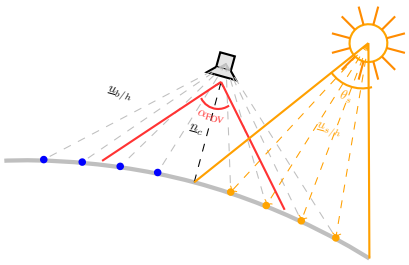

Fig. 2. Visualization of the light emanating from the sun on the points on the surface of the chief satellite: Yellow dots represent inspection points that are illuminated by the sun, while blue dots indicate points that are not illuminated.

Proof: Using the upper bound on the regressor matrix in Assumption 4, the Lie derivative of the candidate Lyapunov function along the flow of (11) is bounded by

$$\dot{V}(\tilde{\theta}_2(t)) \leq \begin{cases} 0, & t < T, \\ -2\underline{a}V(\tilde{\theta}_2(t)), & t \geq T, \end{cases} \tag{12}$$

where $\underline{a} = \lambda_{\min}(\beta)$. At $t < T$, it can be observed from (12) that the observer error $\tilde{\theta}_2(t)$ is non-increasing, specifically $\|\tilde{\theta}_2(t)\| \leq \|\tilde{\theta}_2(0)\|, \forall t < T$. Invoking [21, Theorem 4.10], it can be concluded that the observer error system is exponentially stable and by the Comparison Lemma [21, Lemma 3.4], the bound $\|\tilde{\theta}_2(t)\| \leq \|\tilde{\theta}_2(T)\| e^{-\underline{a}(t-T)}$ holds for all $t \geq T$. ■

IV. Spacecraft Motion Planning under Illumination and FOV Constraints

A. Sun Dynamics and Illumination Constraints

This paper assumes that the Sun is the only light source, confined to the $\vec{x}_H - \vec{y}_H$ plane in Hill's reference frame. The unit vector pointing from the center of the chief satellite to the Sun, denoted by $\underline{u}_{s/h}(t)$, is given by $\underline{u}_{s/h}(t) = \begin{bmatrix} \cos(\theta_s(t)) & \sin(\theta_s(t)) & 0 \end{bmatrix}^\top$, where $\theta_s(t)$ is the angle formed by the conical ray of the sun on the surface of the chief satellite as depicted in Fig. 2. The angle of the sun $\theta_s(t)$ is dependent on the mean motion of the chief satellite n such that [7], [9]

$$\dot{\theta}_s(t) = -n, \quad \theta_s(0) = \theta_{s_0}. \tag{13}$$

Assumption 5: No obstructions are blocking the light emanating from the sun from reaching the chief satellite over the time interval $[0,\ t_f)$. Furthermore, goal locations are selected to ensure that sufficiently many features are illuminated when the deputy spacecraft is at the goal location.

To maximize the number of points within the FOV of the camera, the condition $\cos^{-1}(\langle \underline{p}_{b/h}(t), \underline{n}_c \rangle) \leq \alpha_{\text{FOV}}$ must be satisfied, where the vector $\underline{n}_c \in \mathbb{R}^3$ is normal to the surface of the chief satellite emanating from the centroid of the cluster of features that are currently within the FOV of the camera and the notation $\langle \cdot, \cdot \rangle$ denotes the dot product. This FOV constraint is integrated into the optimal control problem.

B. Information Maximizing Constrained Optimal Control

To facilitate the development of the constrained optimal control problem, let the concatenated vector of the position and velocity of the goal relative to the deputy spacecraft, coordinatized in $\mathcal{F}_\mathcal{H}$, be defined as $\mathbf{x}(t) := \begin{bmatrix} \underline{p}_{g/b}(t)^\top & \underline{v}_{g/b}^\top(t) \end{bmatrix}^\top \in \mathbb{R}^6$. Since the goal is assumed to be stationary relative to the chief satellite, $\underline{v}_{g/b}(t) = \underline{v}_{b/h}(t)$. The linearized CW Dynamics can be then expressed in LTI form as

$$\dot{\mathbf{x}} = A\mathbf{x}(t) + B\mathbf{u}(t), \quad \mathbf{x}(0) = x_0, \tag{14}$$

where $A = \begin{bmatrix} 0 & 0 & 0 & 1 & 0 & 0 \\ 0 & 0 & 0 & 0 & 1 & 0 \\ 0 & 0 & 0 & 0 & 0 & 1 \\ 3n^2 & 0 & 0 & 0 & 2n & 0 \\ 0 & 0 & 0 & -2n & 0 & 0 \\ 0 & 0 & -n^2 & 0 & 0 & 0 \end{bmatrix}$, $B = \frac{1}{m}\begin{bmatrix} 0_{3\times3} \\ I_{3\times3} \end{bmatrix}$, and $\mathbf{u}(t) = \begin{bmatrix} (F)_x & (F)_y & (F)_z \end{bmatrix}^\top \in \mathcal{U}_\mathcal{F} \subset \mathbb{R}^3$, where $\mathcal{U}_\mathcal{F} = \{\mathbf{u} : [0,\ t_f) \to \mathcal{U}_\mathcal{F} : \mathbf{u}(\cdot) \text{ is Lebesgue measurable}\}$ represents the set of admissible controls. Consider a finite horizon continuous-time optimal control problem where the objective is to find an admissible control policy $\mathbf{u} : [0,\ t_f) \to \mathbb{R}^3$ that solves the minimization problem

$$\begin{aligned} &\min_{\mathbf{u}\in\mathcal{U}_\mathcal{F}} \int_0^{t_f} r(\mathbf{x}(\tau), \mathbf{u}(\tau)\, \mathrm{d}\tau + V(\mathbf{x}(t_f), t_f), \\ &\text{s.t.} \quad \nabla_{\mathbf{x}(t)}\Psi(\mathbf{x}(t))\,(A\mathbf{x}(t) + B\mathbf{u}(t)) \leq \alpha(h(\mathbf{x}(t))), \end{aligned} \tag{15}$$

subject to the dynamic constraints in (13) and (14), where $\alpha : \mathbb{R}_{\geq 0} \to \mathbb{R}_{\geq 0}$ is a class $\mathcal{K}$ function and $V : \mathbb{R}^6 \times [0,\ t_f] \to \mathbb{R}_{\geq 0}$ is the terminal cost. The running cost $r : \mathbb{R}^6 \times \mathbb{R}^3 \to \mathbb{R}$ in (15) is defined as $r(\mathbf{x}(t), \mathbf{u}(t)) = \mathbf{x}^\top(t)Q\mathbf{x}(t) + \mathbf{u}^\top(t)R\mathbf{u}(t) + \gamma_c\langle C\mathbf{x}(t), \underline{n}_c\rangle^2$, where $Q \in \mathbb{R}^{6\times6}$, $Q = Q^\top \succ 0$ is the state penalty, $R \in \mathbb{R}^{3\times3}$, $R = R^\top \succ 0$ is the control penalty, $C = \begin{bmatrix} 0_{3\times3} & I_{3\times3} \end{bmatrix} \in \mathbb{R}^{3\times6}$ is a selection matrix, and $\gamma_c \in \mathbb{R}_{>0}$ is a user-defined constant. The term $\gamma_c\langle C\mathbf{x}(t), \underline{n}_c\rangle^2$ is designed to maximize orthogonality of the motion of the camera relative to the normal vector pointing outward from the centroid of the image-plane locations of features currently in the FOV of the camera, denoted by $\underline{n}_c \in \mathbb{R}^3$. The minimization of the dot product $\langle C\mathbf{x}(t), \underline{n}_c\rangle$ is motivated by our earlier findings in [20]. In that study, it was demonstrated that moving the camera orthogonally to the plane containing the features improves the conditioning of the regressor matrix in Assumption 4, thus improving the numerical stability of the ICL-based observer. Since $\gamma_c\langle C\mathbf{x}(t), \underline{n}_c\rangle^2 \equiv \mathbf{x}^\top(t)(\gamma_c C^\top \underline{n}_c \underline{n}_c^\top C)\mathbf{x}(t)$, the running cost defined below (15) can be equivalently expressed as $r(\mathbf{x}(t), \mathbf{u}(t)) = \mathbf{x}^\top(t)\underline{Q}\mathbf{x}(t) + \mathbf{u}^\top(t)R\mathbf{u}(t)$, where $\underline{Q} = Q + \gamma_c C^\top \underline{n}_c \underline{n}_c^\top C$, with $\underline{Q} = \underline{Q}^\top \succ 0$. The barrier-like function $\Psi : \mathbb{R}^6 \to \mathbb{R}_{\geq 0}$ in (15) is defined as

$$\Psi(\mathbf{x}(t)) = (b(\mathbf{x}(t)) - b(0))^2, \tag{16}$$

satisfying $\alpha_1(h(\mathbf{x}(t))) \leq \Psi(\mathbf{x}(t)) \leq \alpha_2(h(\mathbf{x}(t)))$ for all $t \in [0,\ t_f]$ with $\Psi(\mathbf{x}(0)) = 0$, where α_1, α_2 are class $\mathcal{K}$

functions. The function $b : \mathbb{R}^6 \to \mathbb{R}_{\geq 0}$ is a combination of the reciprocal of the constraints defined as $b(\mathbf{x}(t)) = \frac{1}{h(\mathbf{x}(t))} = \sum_{i=1}^{3} \frac{1}{h_i(\mathbf{x}(t))}$, where $h_1 : \mathbb{R}^6 \to \mathbb{R}_{\geq 0}$ is the FOV constraint described above, given by $h_1(\mathbf{x}(t)) = \alpha_{\text{FOV}} - \cos^{-1}(\langle \underline{u}_{b/h}(t), \underline{n}_c(t) \rangle) \geq 0$. The constraint $h_2 : \mathbb{R}^6 \to \mathbb{R}_{\geq 0}$ is designed to ensure that the deputy spacecraft does not collide with the chief satellite, and is given by $h_2(\mathbf{x}(t)) = \sqrt{2a_{\max}(\|\underline{p}_{g/b}(t) + \underline{p}_{g/h}\| - r_{\min})} + \underline{v}_{\text{proj}}(t)$, where $a_{\max}$ is the maximum acceleration from the natural motion and control limits, $r_{\min} = r_d + r_c$ with r_d and $r_c > 0$ representing the radii of the deputy spacecraft and chief satellite, respectively, and $\underline{v}_{\text{proj}}(t) = \langle \underline{v}_{b/h}(t), \underline{p}_{b/h}(t) \rangle / \|\underline{p}_{b/h}(t)\|$. The constraint $h_3 : \mathbb{R}^6 \to \mathbb{R}_{\geq 0}$ is introduced to ensure that the deputy spacecraft stays within the keep-in zone and does not travel too far from the chief satellite, and is given by $h_3(\mathbf{x}(t)) = \sqrt{2a_{\max}(r_{\max} - \|\underline{p}_{g/b}(t) + \underline{p}_{g/h}\|)} + \underline{v}_{\text{proj}}(t)$, where $r_{\max}$ denotes the maximum allowable distance between the deputy spacecraft and the chief satellite (cf. [22]).

C. Optimal Control Design for Inspection

To facilitate the development of the optimal feedback control policy, let $V^* : \mathbb{R}^6 \times [0, t_f] \to \mathbb{R}$ denote the optimal value function which is assumed to be continuously differentiable with $V(t_f, 0) = 0$. The constrained optimization problem in (15) can be converted to an equivalent problem given by the following Hamilton-Jacobi-Bellman (HJB) equation (cf. [23, Equation 27]),

$$0 = \nabla_t V(\mathbf{x}, t) + \min_{\mathbf{u} \in \mathcal{U}_{\mathcal{F}}} \left\{ \nabla_{\mathbf{x}} V(\mathbf{x}, t) \left(A\mathbf{x} + B\mathbf{u} \right) + r(\mathbf{x}, \mathbf{u}) \right\}, \quad \text{s.t.} \quad \nabla_{\mathbf{x}} \Psi(\mathbf{x})(A\mathbf{x} + B\mathbf{u}) \leq \alpha(h(\mathbf{x})). \tag{17}$$

The Lagrangian for the constrained optimization problem in (17) can be expressed as $\mathcal{L}(\mathbf{x}(t), \mathbf{u}(t), \lambda, t) = \nabla_{\mathbf{x}(t)} V(\mathbf{x}(t), t)(A\mathbf{x}(t) + B\mathbf{u}(t)) + r(\mathbf{x}(t), \mathbf{u}(t)) + \lambda[\nabla_{\mathbf{x}(t)} \Psi(\mathbf{x}(t))(A\mathbf{x}(t) + B\mathbf{u}(t)) - \alpha(h(\mathbf{x}(t)))]$, for all $\mathbf{x}(t) \in \mathbb{R}^6$ and $t \in [0, t_f)$, where λ denotes the Lagrange multiplier. The optimal control policy can be obtained by solving the Karush–Kuhn–Tucker conditions [23], [24] for the constrained optimization problem, which provides the following necessary conditions for optimality

$$2\mathbf{u}^\top(t)R + \left(\nabla_{\mathbf{x}(t)} V(\mathbf{x}(t), t) + \lambda \nabla_{\mathbf{x}(t)} \Psi(\mathbf{x}(t)) \right) B = 0, \tag{18}$$

$$\nabla_{\mathbf{x}(t)} \Psi(\mathbf{x}(t))(A\mathbf{x}(t) + B\mathbf{u}(t)) - \alpha(h(\mathbf{x}(t))) \leq 0, \tag{19}$$

$$\lambda \left(\nabla_{\mathbf{x}(t)} \Psi(\mathbf{x}(t))(A\mathbf{x}(t) + B\mathbf{u}(t)) - \alpha(h(\mathbf{x}(t))) \right) = 0, \tag{20}$$

$$\lambda \geq 0. \tag{21}$$

By substituting u in (18) into the complementary slackness condition in (20) and using the condition on the dual constraint in (21), the optimal Lagrange multiplier for the optimal solution of (15) can be expressed as (cf . [25])

$$\lambda^*(t) = \begin{cases} \frac{S(\mathbf{x}(t), t)}{\mathcal{R}_B(\mathbf{x}(t))}, & \text{if } \mathcal{R}_B(\mathbf{x}(t)) \neq 0 \\ & \text{and } S(\mathbf{x}(t), t) > 0, \\ 0, & \text{otherwise}, \end{cases} \tag{22}$$

where $S(\mathbf{x}(t), t) = 2(\nabla_{\mathbf{x}(t)} \Psi(\mathbf{x}(t)) A\mathbf{x}(t) - \frac{1}{2} \nabla_{\mathbf{x}(t)} \Psi(\mathbf{x}(t)) R_B \nabla_{\mathbf{x}(t)} (V^*(\mathbf{x}(t), t))^\top - \alpha(h(\mathbf{x}(t))))$, $\mathcal{R}_B(\mathbf{x}(t)) = \nabla_{\mathbf{x}(t)} \Psi(\mathbf{x}(t)) R_B \nabla_{\mathbf{x}(t)} \Psi^\top(\mathbf{x}(t))$, and $R_B = BR^{-1}B^\top$. By solving the stationarity condition in (18), the optimal controller is given by the feedback policy $\mathbf{u}^* : \mathbb{R}^6 \times [0,\ t_f] \to \mathbb{R}^3$ computed as

$$\mathbf{u}^*(\mathbf{x}(t), t) = -\frac{1}{2} R^{-1} B^\top \nabla_{\mathbf{x}(t)} \left(V^*(\mathbf{x}(t), t) \right)^\top - \frac{1}{2} R^{-1} B^\top \lambda^*(t) \nabla_{\mathbf{x}(t)} \Psi^\top(\mathbf{x}(t)). \tag{23}$$

In the following, the terminal cost of the constrained optimal control problem in (15) is selected to be $V(\mathbf{x}(t_f), t_f) \coloneqq \mathbf{x}^\top(t_f) Q_f \mathbf{x}(t_f)$, with $\nabla_{\mathbf{x}(t_f)} V(\mathbf{x}(t_f)) = 2Q_f \mathbf{x}(t_f)$, where $Q_f = Q_f^\top \succ 0$ is a user-selected penalty matrix. The near-optimal approximate control policy is designed as (cf. [26])

$$\mathbf{u}(t) = -R^{-1} B^\top P(t) \hat{\mathbf{x}}(t) - \frac{k_s}{2} R^{-1} B^\top \nabla_{\hat{\mathbf{x}}(t)} \Psi^\top(\hat{\mathbf{x}}(t)), \tag{24}$$

where $\hat{\mathbf{x}}(t)$ is the estimate of $\mathbf{x}(t)$ and $P(t)$ is the solution of the Ricatti differential equation associated with the CW linear dynamics in (14), given by,

$$\dot{P}(t) = -A^\top P(t) - P(t)A + P(t) B R^{-1} B^\top P(t) + \underline{Q}, \tag{25}$$

with terminal condition $P(t_f) = \underline{Q}_f$, where $\underline{Q}_f = Q_f + \gamma_c C^\top \underline{n}_c \underline{n}_c^\top C$ and $\underline{Q}_f = \underline{Q}_f^\top \succ 0$. The solution $P(t)$ satisfies $\underline{p} I_{6\times 6} \leq P(t) \leq \overline{p} I_{6\times 6}$ for all $t \in [0, t_f]$, where $\underline{p}$, and $\overline{p} > 0$ are constant bounds. The constant $k_s > 0$ is a user-selected constant chosen to estimate the optimal Lagrange multiplier.

V. Stability Analysis of the Spacecraft

This section presents the Lyapunov-based stability analysis of the system in (14), under the feedback control law in (24). To facilitate the analysis, let $V_L : \mathbb{R}^6 \times [0,\ t_f] \to \mathbb{R}$ be a candidate Lyapunov function defined as

$$V_L(\mathbf{x}(t), t) = \frac{1}{2} \mathbf{x}^\top(t) P(t) \mathbf{x}(t) + k_s \Psi(\mathbf{x}(t)), \tag{26}$$

which satisfies the following bound given that $P(t)$ and $\Psi(\mathbf{x}(t))$ are bounded $\underline{v}_l \|\mathbf{x}(t)\|^2 \leq V_L(\mathbf{x}(t), t) \leq \overline{v}_l \|\mathbf{x}(t)\|^2$, for all $t \in [0,\ t_f]$ and for all $\mathbf{x}(t) \in \mathbb{R}^6$, where $\underline{v}_l$ and $\overline{v}_l > 0$ are constants. The barrier-like function Ψ is assumed to be locally Lipschitz continuous on a compact ball $\overline{B}(0, \chi)$ of radius $\chi > 0$ centered at the origin. Since the ICL observer error system in (11) is exponentially stable and since $\underline{u}_{g/b}(t)$ being a unit vector implies that $\|\underline{u}_{g/b}(t)\| = 1$, it holds that $\|\mathbf{x}(t) - \hat{\mathbf{x}}(t)\| = \|\underline{p}_{g/b}(t) - \hat{\underline{p}}_{g/b}(t)\| \leq \|\underline{d}_{g/b}(0) - \hat{\underline{d}}_{g/b}(0)\| \leq \epsilon_d$, where the bound $\epsilon_d > 0$ is a constant. Let $\mathcal{C} \subset \mathbb{R}^6$ be a compact set defined as $\mathcal{C} \coloneqq \{\mathbf{x}(t) \in \mathbb{R}^6 : \|\mathbf{x}(t)\| + \epsilon_d \leq \chi\}$. Since Ψ is locally Lipschitz continuous on $\mathcal{C}$ and $\mathcal{C}$ is compact, there exists a Lipschitz constant $L_\Psi > 0$ such that $\Psi(\mathbf{x}(t)) - \Psi(\hat{\mathbf{x}}(t)) \leq L_\Psi \|\mathbf{x}(t) - \hat{\mathbf{x}}(t)\|$, for all $\mathbf{x}(t), \hat{\mathbf{x}}(t) \in \mathcal{C}$.

Theorem 2: Let $r > 0$ be such that $\overline{B}(0, r) \subset \mathcal{C}$. Provided Assumptions 1–4 hold and the barrier-like function Ψ is locally Lipschitz continuous on $\overline{B}(0, \chi)$, if the sufficient conditions

$$k_s \geq \sqrt{\frac{9(2k_s \overline{p} \lambda_{\max}(R_B) + k_s \|A\|)^2}{4\lambda_{\min}(\underline{Q}) \lambda_{\min}(R_B)}}, \quad \sqrt{\frac{\underline{v}_l}{\kappa}} < \sqrt{\frac{\overline{v}_l}{\underline{v}_l}} r^2, \tag{27}$$

are satisfied, where $R_B = BR^{-1}B^\top$, and if the distance estimates are updated using the adaptive update law defined in (10), then the trajectories of the system in (14), $\mathbf{x}(t)$, is locally uniformly ultimately bounded (UUB) under the control policy designed in (24).

Proof: The Lie derivative of the candidate Lyapunov function V_L along the flow of (14) is bounded on $\mathcal{C}$ by

$$\dot{V}_L(\mathbf{x}(t),t) = -\lambda_{\min}(\underline{Q})\left\|\mathbf{x}(t)\right\|^2 + \varpi_1\left\|\mathbf{x}(t)\right\| - k_s^2\lambda_{\min}(R_B)\left\|\nabla_{\mathbf{x}(t)}\Psi(\mathbf{x}(t))\right\|^2 + \varpi_2\left\|\nabla_{\mathbf{x}(t)}\Psi(\mathbf{x}(t))\right\| + \varpi_3\left\|\nabla_{\mathbf{x}(t)}\Psi(\mathbf{x}(t))\right\|\left\|\mathbf{x}(t)\right\|, \quad (28)$$

where $\varpi_1 = 2\overline{p}^2\lambda_{\max}(R_B)\epsilon_d + k_s\overline{p}\lambda_{\max}(R_B)L_\Psi\epsilon_d$, $\varpi_2 = 2k_s^2\lambda_{\max}(R_B)L_\Psi\epsilon_d + k_s\overline{p}\lambda_{\max}(R_B)\epsilon_d$, and $\varpi_3 = 2k_s\overline{p}\lambda_{\max}(R_B) + k_s\|A\|$. Applying completion of squares and letting $\kappa = \frac{1}{2}\min\left\{\frac{\lambda_{\min}(\underline{Q})}{3}, \frac{k_s^2\lambda_{\min}(R_B)}{3}\right\}$ and $\iota = \frac{3\varpi_1^2}{4\lambda_{\min}(\underline{Q})} + \frac{3\varpi_2^2}{4k_s^2\lambda_{\min}(R_B)}$, and provided the first gain condition in (27) is satisfied, then the bound in (28) can be expressed as $\dot{V}_L(\mathbf{x}(t),t) \leq -\kappa\left(\left\|\mathbf{x}(t)\right\|^2 - \frac{\iota}{\kappa}\right)$, which implies that $\dot{V}_L$ is negative definite for all $\left\|\mathbf{x}(t)\right\| > \sqrt{\frac{\iota}{\kappa}} > 0$ and for all $\mathbf{x}(t) \in \overline{B}(0,r) \subset \mathcal{C}$. Hence, provided both sufficient conditions stated in (27) and the bound on V_L are satisfied, [21, Theorem 4.18] can be invoked to conclude that for every trajectory $\mathbf{x}(t)$ satisfying $\left\|\mathbf{x}(0)\right\| \leq \sqrt{\frac{\overline{\upsilon}_l}{\underline{\upsilon}_l}r^2}$, there is $T \geq 0$ (dependent on $\mathbf{x}(0)$ and $\sqrt{\frac{\iota}{\kappa}}$) such that $\left\|\mathbf{x}(t)\right\| \leq \sqrt{\frac{\overline{\upsilon}_l}{\underline{\upsilon}_l}\left(\frac{\iota}{\kappa}\right)}$, $\forall t \geq T$. Hence, the concatenated state, $\mathbf{x}(t)$, is locally uniformly ultimately bounded under the controller designed in (24). ∎

VI. Conclusion

This paper solves the on-orbit inspection problem, where a deputy spacecraft is tasked with navigating safely within the orbital environment while inspecting the features of a chief satellite in the presence of illumination and FOV constraints. To achieve better conditioning of the regressor matrix of the ICL-based distance observer used to create a local map of the chief satellite, a cost function that maximizes information gain from the camera is added to the running cost of a receding horizon optimal control problem. Future work will explore relaxing some of the assumptions made in the paper and include more complex estimation objectives such as 3-dimensional shape reconstruction.

References

[1] D. Fourie, B. E. Tweddle, S. Ulrich, and A. Saenz-Otero, "Flight results of vision-based navigation for autonomous spacecraft inspection of unknown objects," *J. Spacecraft Rockets*, vol. 51, no. 6, pp. 2016–2026, 2014.

[2] J. A. Placed, J. Strader, H. Carrillo, N. Atanasov, V. Indelman, L. Carlone, and J. A. Castellanos, "A survey on active simultaneous localization and mapping: State of the art and new frontiers," *IEEE Trans. Robot.*, vol. 39, no. 3, pp. 1686–1705, 2023.

[3] Y. K. Nakka, W. Hönig, C. Choi, A. Harvard, A. Rahmani, and S.-J. Chung, "Information-based guidance and control architecture for multi-spacecraft on-orbit inspection," *J. Guid. Control Dynam.*, vol. 45, no. 7, pp. 1184–1201, 2022.

[4] J. A. Starek, E. Schmerling, G. D. Maher, B. W. Barbee, and M. Pavone, "Fast, safe, propellant-efficient spacecraft motion planning under Clohessy–Wiltshire–Hill dynamics," *J. Guid. Control Dynam.*, vol. 40, no. 2, pp. 418–438, 2017.

[5] R. Volpe, C. Circi, M. Sabatini, and G. B. Palmerini, "GNC architecture for an optimal rendezvous to an uncooperative tumbling target using passive monocular camera," *Acta Astronaut.*, vol. 196, pp. 380–393, 2022.

[6] M. Maestrini and P. Di Lizia, "Guidance strategy for autonomous inspection of unknown non-cooperative resident space objects," *J. Guid Control Dynam.*, vol. 45, no. 6, pp. 1126–1136, 2022.

[7] D. van Wijk, K. Dunlap, M. Majji, and K. L. Hobbs, "Deep reinforcement learning for autonomous spacecraft inspection using illumination," arXiv:2308.02743, 2023.

[8] C. Choi, Y. K. Nakka, A. Rahmani, and S.-J. Chung, "Resilient multi-agent collaborative spacecraft inspection," in *Proc. IEEE Aerosp. Conf.*, 2023, pp. 1–10.

[9] C.-K. McQuinn, K. Dunlap, N. Hamilton, J. Wilson, and K. L. Hobbs, "Run time assurance for simultaneous constraint satisfaction during spacecraft attitude maneuvering," arXiv:2402.14723, 2024.

[10] D. Akhihiero, U. Olawoye, S. Das, and J. Gross, "Cooperative localization for GNSS-denied subterranean navigation: A UAV–UGV team approach," *J. Inst. Navig.*, vol. 71, no. 4, 2024.

[11] M. Schwager, J.-J. Slotine, and D. Rus, "Unifying geometric, probabilistic, and potential field approaches to multi-robot coverage control," in *Robotics Research*, C. Pradalier, R. Siegwart, and G. Hirzinger, Eds. Berlin, Heidelberg: Springer Berlin Heidelberg, 2011, pp. 21–38.

[12] M. Schwager, B. J. Julian, M. Angermann, and D. Rus, "Eyes in the sky: Decentralized control for the deployment of robotic camera networks," *Proc. IEEE*, vol. 99, no. 9, pp. 1541–1561, 2011.

[13] B. E. Tweddle and A. Saenz-Otero, "Relative computer vision-based navigation for small inspection spacecraft," *J. Guid. Control Dynam.*, vol. 38, no. 5, pp. 969–978, 2015.

[14] Y. Ma, S. Soatto, J. Kosecka, and S. S. Sastry, *An invitation to 3-D vision*. Springer, 2004.

[15] J.-Y. Bouguet, "Pyramidal implementation of the affine lucas kanade feature tracker description of the algorithm," *Intel corporation*, vol. 5, no. 1-10, p. 4, 2001.

[16] B. Lucas and T. Kanade, "An iterative image registration technique with an application to stereo vision," in *Proc. Int. Joint Conf. Artif. Intell.*, 1981, pp. 674–679.

[17] J. B. MacQueen, "Some methods for classification and analysis of multivariate observations," *Proc. 5th Berkeley Symp. Math. Stat. Prob.*, vol. 1, 1967.

[18] Z. I. Bell, H.-Y. Chen, A. Parikh, and W. E. Dixon, "Single scene and path reconstruction with a monocular camera using integral concurrent learning," in *Proc. IEEE Conf. Decis. Control*. IEEE, 2017, pp. 3670–3675.

[19] Z. I. Bell, P. Deptula, E. A. Doucette, J. W. Curtis, and W. E. Dixon, "Simultaneous estimation of Euclidean distances to a stationary object's features and the Euclidean trajectory of a Monocular camera," *IEEE Trans. Autom. Control*, vol. 66, no. 9, pp. 4252–4258, 2020.

[20] T. E. Ogri, M. Qureshi, Z. I. Bell, K. Waters, and R. Kamalapurkar, "An adaptive optimal control approach to monocular depth observability maximization," in *Proc. Am. Control Conf.*, 2024.

[21] H. K. Khalil, *Nonlinear systems*, 3rd ed. Upper Saddle River, NJ: Prentice Hall, 2002.

[22] K. Dunlap, D. van Wijk, and K. L. Hobbs, "Run time assurance for autonomous spacecraft inspection," arXiv: 2302.02885, 2023.

[23] V. Nevistic and J. A. Primbs, "Constrained nonlinear optimal control: a converse HJB approach," California Institute of Technology, Pasadena, CA 91125, Tech. Rep. CIT-CDS 96-021, 1996.

[24] A. E. Bryson and Y. Ho, *Applied optimal control: optimization, estimation, and control*. Hemisphere Publishing Corporation, 1975.

[25] L. Sforni, G. Notarstefano, and A. D. Ames, "Receding horizon CBF-based multi-layer controllers for safe trajectory generation," in *Proc. Am. Control Conf.*, 2024, pp. 4765–4770.

[26] S. Bandyopadhyay and S. Bhasin, "Safe Q-Learning for continuous-time linear systems," in *Proc. IEEE Conf. Decis. Control*, 2023, pp. 241–246.